Applied Catalysis B: Environment and Energy 347 (2024) 123793

Contents lists available at ScienceDirect

Applied Catalysis B: Environment and Energy

journal homepage: www.elsevier.com/locate/apcatb

New insight into the activation mechanism of peroxymonosulfate by N, O-doped carbonaceous materials: Active sites, intermediates, and pathways

Jingjing Yang [a,b], Joseph Pignatello [c,*], Chen Yang [b], Yi Yang [d], Zhengyang Wang [c], Rui Wang [e], Kejia Zhang [a], Chengjin Wang [c,g], Zhi Dang [b], Qing Zhao [a,*], Fengchang Wu [f]

[a] Guangdong Key Laboratory of Integrated Agro-environmental Pollution Control and Management, Institute of Eco-environmental and Soil Sciences, Guangdong Academy of Sciences, Guangzhou 510650, China
[b] School of Environment and Energy, South China University of Technology, Guangzhou 510006, China
[c] The Connecticut Agricultural Experiment Station, New Haven, CT 06511, United States
[d] CAS Key Laboratory of Urban Pollutant Conversion, Department of Environmental Science and Engineering, University of Science and Technology of China, Hefei 230026, China
[e] State Environmental Protection Key Laboratory of Environmental Pollution Health Risk Assessment, South China Institute of Environmental Sciences, Ministry of Ecology and Environment, Guangzhou 510655, China
[f] State Key Laboratory of Environmental Criteria and Risk Assessment, Chinese Research Academy of Environmental Sciences, Beijing 100012, China
[g] Department of Civil Engineering, University of Manitoba, Winnipeg, Manitoba R3T 5V6, Canada

ARTICLE INFO

Keywords:
Carbonaceous materials
Peroxymonosulfate
Activation mechanism
Active intermediate
Reaction pathway

ABSTRACT

Persulfates activation by N,O-doped carbonaceous materials is an emerging advanced oxidation process for removing organic pollutants from water. However, the specific activation mechanisms including active sites, intermediates, and pathways are unknown. We prepared a N,O-doped carbocatalyst (NOGM) as model material to unveil the activation mechanism. Reaction occurred on the surface. After ruling out oxyl radicals, singlet oxygen, persistent free radicals, and through-surface direct electron transfer, a two-electron (nucleophilic-electrophilic) reaction involving short-lived bound PMS species or PMS-transformed surface groups was found to be the most likely pathway. Pre-contact of NOGM with PMS generates bound -OO- groups and causes major transformations of surface functionality identified in unprecedented detail. Results indicate that imine-type edge-N (A-1 and A′−1) would be the possible active sites and oxaziridine (neutral and charged) is possible active intermediates. Activation pathways are proposed. This study goes far in providing a strategy for designing new carbonaceous materials with high efficiency for activation peroxides.

1. Introduction

Water pollution by organic chemicals has become a serious problem threatening ecological and human health. Peroxymonosulfate (PMS; HSO_5^-) is an inexpensive and efficient bulk oxidant in advanced oxidation processes (AOPs) for treating organic contaminated water. Since PMS is itself a weak oxidant, its successful use normally requires activation by heat, ultraviolet light, reduced metal ions, metal oxide catalysts, or carbocatalysts [47,53,54]. Many studies used metal-free carbonaceous materials for PMS activation including carbon nanotubes [16,22,62,67], graphene [12,41], reduced graphene oxide [40], nanodiamond [13,23,35], hierarchically porous carbons, [64] and biochars [14,46,48] due to their intrinsic properties such as no-metal leaching, acid/alkaline resistance, and versatility. However, the pathways of PMS activation by metal-free carbonaceous materials and subsequent organic compound oxidation are still under debate.

Proposed reaction pathways include surface-mediated generation of oxyl radicals (•OH and SO_4•$^-$) [11,13,10,3] or singlet oxygen ($^1O_2$) [24,30]), surface-mediated electron transfer between the organic compound and PMS [23,42,63,61,65], and formation of PMS in an activated state (PMS*) on the surface [30,63]. Evidence for these pathways is often based on qualitative or semi-quantitative observations, such as detection of electron paramagnetic resonance (EPR) signals; inhibition (or lack-thereof) by ROS scavengers; formation of specific probe byproducts; appearance of current in an electrochemical cell where reactants are compartmented; substrate structure-reactivity patterns; comparison of reaction intermediates; or trends in PMS consumption with and without target compound. Seldom is an activation pathway identified by

* Corresponding authors.
E-mail addresses: joseph.pignatello@ct.gov (J. Pignatello), zhaoqing@iae.ac.cn (Q. Zhao).

https://doi.org/10.1016/j.apcatb.2024.123793
Received 17 November 2023; Received in revised form 19 January 2024; Accepted 29 January 2024
Available online 1 February 2024

quantitative measures. Recent observations proposed that carbonaceous materials, especially those pyrolyzed at high temperatures, mediate oxidation of organic compounds by peroxydisulfate (PDS) by nonradical pathways [33,36,65,8]. Compared to radical-based oxidation, non-radical oxidation of pollutants features advantages of minimal water matrix interference, maximum use of oxidants, and prevention of radical self-quenching [15,49,55]. Therefore, an understanding the specific process of non-radical oxidation is of significance for the practical application of persulfate-based advanced oxidation systems.

A central question about persulfate activation by carbonaceous materials is the nature of active sites and active intermediates. Answering this question is critical for improving catalyst performance and understanding degradation pathways, but is hindered by the complexity and heterogeneity of carbocatalyst materials.

Oxygen functional groups, structural defects, and the heteroatoms of carbocatalysts have variously been proposed as PMS activation sites. Quinone [68] and ketone [35] groups were regarded as active sites for $^1O_2$ production. Defect sites where activation is suggested to occur include zigzag edges and vacancies [9,10]. Nitrogen-doping has been identified as a means of increasing activity. N-doping is said to create Lewis base sites that can participate in redox processes. [17] Thermal evaporation of the N dopant is thought to create topological defects that may participate in redox processes [52,58,66]. It has also been proposed that unsaturated carbon atoms at edge sites can participate in the redox process [50]. It remains unclear exactly how these sites activate PMS and exactly what the active oxidant species is that attacks the organic compound. Detection of a specific species does not necessarily mean it is a major contributor to target compound degradation. Correlations between degradation rate constants and the content of specific nitrogen species (graphitic N [10] , pyridinic and pyrrolic N [27]) have been offered as evidence for their respective role in PMS activation. However, no clear picture has emerged. Assignment of mechanism is hindered by the current inability to produce carbons with a single type of heterocyclic N and uniform conjugated ring size. The decisive role of surface chemistry on the activation properties of carbon materials has long been recognized.

To address the aforementioned critical uncertainties, we prepared a highly-active N,O-doped carbonaceous material and used it as a model for exploring the activation mechanism of PMS. A set of advanced techniques including in-situ Raman, operando diffuse reflectance infrared Fourier transform spectroscopy (DRIFTS), X-ray photoelectron spectroscopy (XPS), and X-ray absorption spectroscopy (XAFS) were applied to explore the actives sites and corresponding active intermediates. The findings of this study can provide information critical for the design of highly-efficient carbocatalysts.

2. Materials and Methods

2.1. Preparation and characterization of materials

Sources of the reagents appear in the Supplemental Section, Text S1A. NOGM was prepared by pyrolysis of a 10:1 (w:w) mixture of melamine and glucose heated to 550 °C and then to 800 °C [25]. A glucose char control was prepared similarly and labeled GC. A schematic, method details, and a cautionary statement about fumes generated during pyrolysis are in Text S1B. Methods of characterization are detailed in Text S1C. X-ray adsorption spectra of NOGM, NOGM reacted with PMS (NOGM-PMS) and chemical were recorded at Soft X-Ray Magnetic Circular Dichroism Endstation (MCD-A and MCD-B), National Synchrotron Radiation Laboratory, University of Science and Technology of China, detailed in Text S1C and Figs. S1 and S2.

2.2. Degradation procedures

Degradation performance was evaluated using conical flasks containing 100 mL of phosphate-buffered (50 mM; pH 7 ± 0.1) ultrapure water (> 18 MΩ cm; Milli-Q system). Test solid was added followed by a small volume of test compound stock solution and the flask was agitated (orbital shaker, 100 rpm) in the dark at 20 ± 0.5 ℃ for a sorption period of 60 min, sufficient to achieve steady-state concentration of 2,4-DCP (Fig. S3). Reaction was initiated by adding a small volume of aqueous Oxone® to reach the desired initial PMS concentration, and agitation continued. Aliquots (~1 mL) were withdrawn by syringe at intervals, filtered through a 0.22 μm PTFE filter (Whatman), and combined with 10 μL of 2 M $Na_2S_2O_3$ to destroy the remaining PMS. Reactant concentrations are given in figure captions. Preliminary experiments showed no effect of buffer concentration (5–50 mM) on rate. Some experiments involved pre-contacting NOGM with PMS solution for different times before adding test compound. The Electrochemical Cell Experiment is described in Text S1D.

2.3. Analytical and Calculation Methods

Concentration of organic compounds were determined by high-performance liquid chromatography with UV detection. PMS was determined by the 2,2′-azino-bis(3-ethylbenzothiazoline-6-sulfonic acid) diammonium salt (ABTS) method [59] (Text S1E). Degradation products were extracted from the solids by methanol and analyzed by liquid chromatography-mass spectrometry (LC-MS, QTOF) equipped with an electron spray ionization source, as described in Text 1 F. DFT calculations are described in Text S2.

3. Results and Discussion

3.1. Rate Law and Effects of Reaction Conditions

Activation performance was tested with phenol, three chlorinated phenols (4-CP, 2,4-DCP and 2,4,6-TCP), 4-nitrophenol (4-NP), bisphenol-A, benzoic acid, carbamazepine, and sulfamethazine using 3 mg/100 mL NOGM at pH 7 (Fig. 1a). After the 60-min sorptive pre-equilibration period, the test compounds reacted with 1 mM PMS at rates that followed the order, Sulfamethazine (0.0896 min^{-1}) > Phenol (0.0659 min^{-1}) > 4-CP (0.0484 min^{-1}) > 2,4-DCP (0.0432 min^{-1}) > 2,4,6-TCP (0.0424 min^{-1}) > bisphenol-A (0.0223 min^{-1}) > 4-NP (0.009 min^{-1}). At 0.1 g/L NOGM, 2,4-DCP was completely removed within < 10 min. Carbamazepine and benzoic acid did not react within 2 h indicating that selectivity of NOGM-PMS. We have examined the correlations between the physical-chemical properties of the compounds listed in Table S2 and their degradation rates. However, no clear correlations were identified. This lack of correlation could be attributed to the dissociation or partial dissociation of some compounds at pH 7, such as 4-nitrophenol (p*K*a = 7.15), benzoic acid (p*K*a = 4.2), and sulfamethazine (p*K*a = 2.65/7.65) because the redox potential of these dissociated forms may differ significantly from their undissociated counterparts.

2,4-DCP was selected to probe reaction kinetics because its degradation rate is intermediate among the compounds tested. It provides a convenient reaction timeframe and allows accurate rate data at low conversion. Inspection of Fig. 1a, S1, and S4 shows that the timescales of 2,4-DCP sorption and reaction are comparable—i.e., complete within minutes or a few tens of minutes. Thus, a rate constant derived from the aqueous 2,4-DCP decay curve reflects a combination of chemical reaction and redistribution between solid and liquid phases in response to the drop in overall concentration. Fig. S5a shows clearly that the rate of aqueous 2,4-DCP decay at constant (and excess) PMS (1 mM) and constant NOGM (3 mg/100 mL) declines with increasing initial 2,4-DCP concentration (0.01 to 0.2 mM). This means that 2,4-DCP decay is less than first-order in $[2,4\text{-DCP}]_{aq}$, otherwise the curves would closely overlap.

Because simple first-order decay laws do not apply, we applied the method of initial rates (MIR) to determine reaction orders in $[2,4\text{-DCP}]_{aq}$ and $[PMS]_{aq}$. Using the MIR also allows us to disregard depletion of the

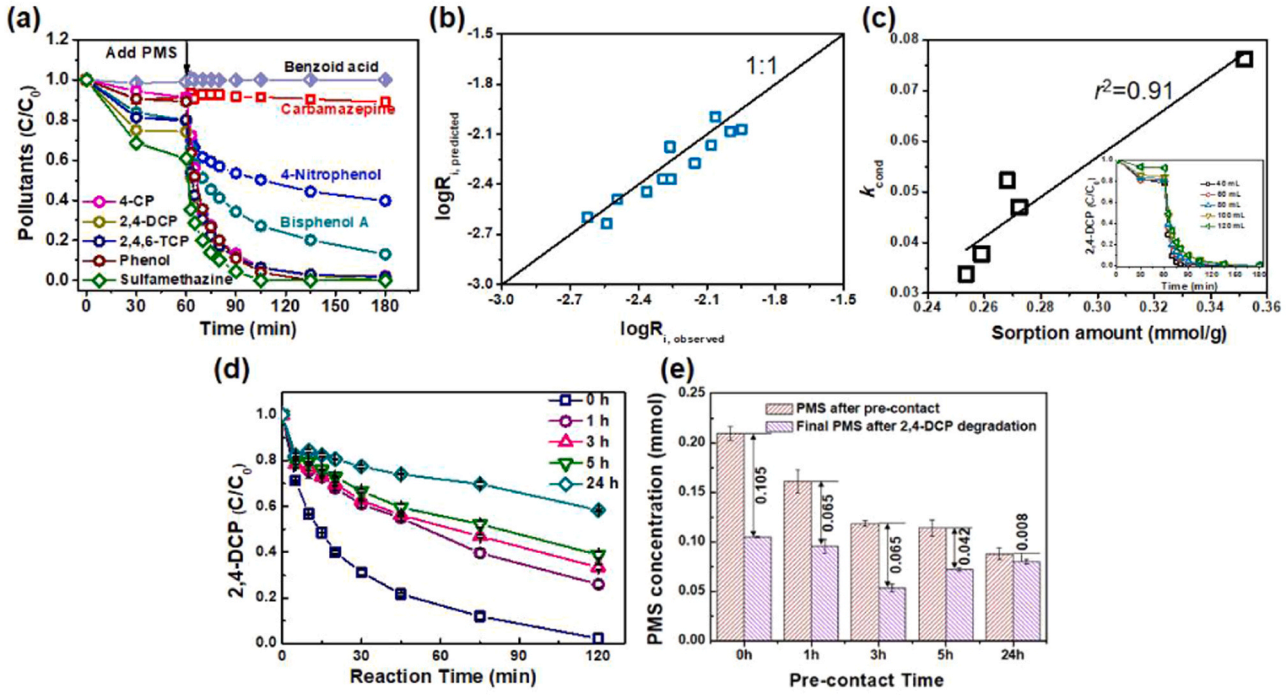

Fig. 1. (a) Degradation curves of different pollutants by PMS activated by NOGM, $[\text{Pollutants}]_0 = 50$ μM, NOGM= 3 mg/100 mL, $[\text{PMS}]_0 = 1$ mM; (b) correlation between observed and predicted logR_i; (c) correlation between k_{cond} and sorption amount of 2,4-DCP in systems with different volumes; (d) 2,4-DCP degradation curves in the NOGM/PMS systems pre-contact for different time; (e) PMS concentrations in the NOGM/PMS systems pre-contact for different time before and after degradation, NOGM= 3 mg/100 mL, $[\text{PMS}]_0 = 0.2$ mM, $[\text{2,4-DCP}]_0 = 50$ μM. pH= 7.

co-reactant during degradation. The overall rate law can be written,

$$R = -\frac{d[2,4-\text{DCP}]_{\text{aq}}}{dt} = k_{cond}\cdot[2,4-\text{DCP}]_{\text{aq}}^{\ x}[\text{PMS}]_{aq}^{y} \quad (1)$$

where t is reaction time after PMS addition; x and y are the reaction orders in 2,4-DCP and PMS, respectively; and k_{cond} is a conditional rate constant which is dependent on the contributions of both diffusion and reaction. Eq. 1 may be transformed to Eq. 2:

$$\log R_i = \log k_{cond} + x \log [2,4-\text{DCP}]_{aq,i} + y \log [\text{PMS}]_{aq,i} \quad (2)$$

where i represents the "initial" value at t close to 0.

R_i for each decay curve was evaluated by fitting the data points to an empirical dual-exponential function and R_i was taken to be the mean of the first derivative (slope) of that function calculated at 90–99% (unit increments) of $[\text{2,4-DCP}]_{\text{aq},t=0}$ and applied to the value computed at $0.95[\text{2,4-DCP}]_{\text{aq},t=0}$, as described in Text S3. The R_i values thus obtained from the decay curves in Fig. S5a (variable 2,4-DCP and constant excess PMS) and Fig. S5b (constant 2,4-DCP and variable excess PMS) were regressed according to Eq. 2, yielding $x = 0.61 \pm 0.10$ (r^2 =0.88), and $y = 0.30 \pm 0.01$ (r^2 =0.99). A plot of observed vs predicted log R_i appears in Fig. 1b.

Fig. 1b shows that the conditional orders in 2,4-DCP (x=0.61) and PMS (y=0.30) are considerably below 1. This can be explained, at least in part, by assuming the rate is governed by the surface concentrations of 2,4-DCP and either PMS itself or a PMS-derived active site. Equilibrium sorption by carbonaceous solids is typically nonlinear with respect to solute concentration, often obeying a power-law model such as the Freundlich ($S = K_F C^n$, where S and C are the equilibrium sorbed and solution concentrations, K_F is the sorption coefficient, and n is an exponent), where n is commonly well below 1. The pre-equilibrium data in Figs. S4b, Fig. S5a, and Fig. S5b can be used to construct a 1-h sorption isotherm for 2,4-DCP (Fig. S6). When fitted to the Freundlich model, n is found equal to 0.49 ± 0.03, which is similar in magnitude to x from Eq. 2. The nonlinear dependence of rate on $[\text{PMS}]_{\text{aq,i}}$ has a more complex explanation because PMS is decomposed by the catalyst (discussed later).

An experiment was performed to test how k_{cond} relates to 2,4-DCP sorbed concentration. It was designed to compare reactors with NOGM exposed to identical conditions except the fraction of 2,4-DCP initially sorbed, which was adjusted by varying solution volume. Vessels containing identical mass of NOGM (3 mg) were equilibrated for 1 h with different volumes (40–100 mL) of initially 50 μM 2,4-DCP. The fraction sorbed increases with solution volume under these conditions. The mixtures were then spiked with PMS to achieve the same initial dissolved concentration of 1 mM PMS in each vessel. The k_{cond} were calculated by the MIR. Fig. 1c shows that k_{cond} correlates with the sorbed concentration of 2,4-DCP, proving that reaction takes place on/near the surface. Fig. S7 and accompanying discussion address the effects of components in environmental waters on 2,4-DCP degradation rates.

3.2. Reactive species identification

3.2.1. Exclusion of ROS and long-range surface-mediated electron transfer

A major role for $SO_4^{\cdot-}$ or HO· as well as singlet oxygen can be ruled out based on the alcohol scavenging experiments (Fig. 2a), lack of reactivity of benzoate and carbamazepine (Fig. 1a), and negligible kinetic solvent isotope effect (Fig. 2b). Despite the low impedance of NOGM compared to GC, long-range surface-mediated electron transfer is minor for the following reasons: 1) The negligible reactivity observed when the reactants are separated in an electrochemical cell (Fig. 2c); 2) because electrons are transferred singly, not in pairs, an electron transferred from pollutant to PMS along the surface would certainly generate $SO_4^{\cdot-}$ or HO·, which we know do not contribute appreciably to 2,4-DCP oxidation; 3) one-electron transfer from 2,4-DCP to PMS is thermodynamically unfavorable in aqueous solution, and physisorption alone is unlikely to alter the electronic structures of either species sufficiently to make it favorable. Although a strong EPR signal (g-factor = 2.0031) which assigned to either carbon-centered radicals with an adjacent heteroatom, or a mixture of carbon- and oxygen-centered radicals [43,

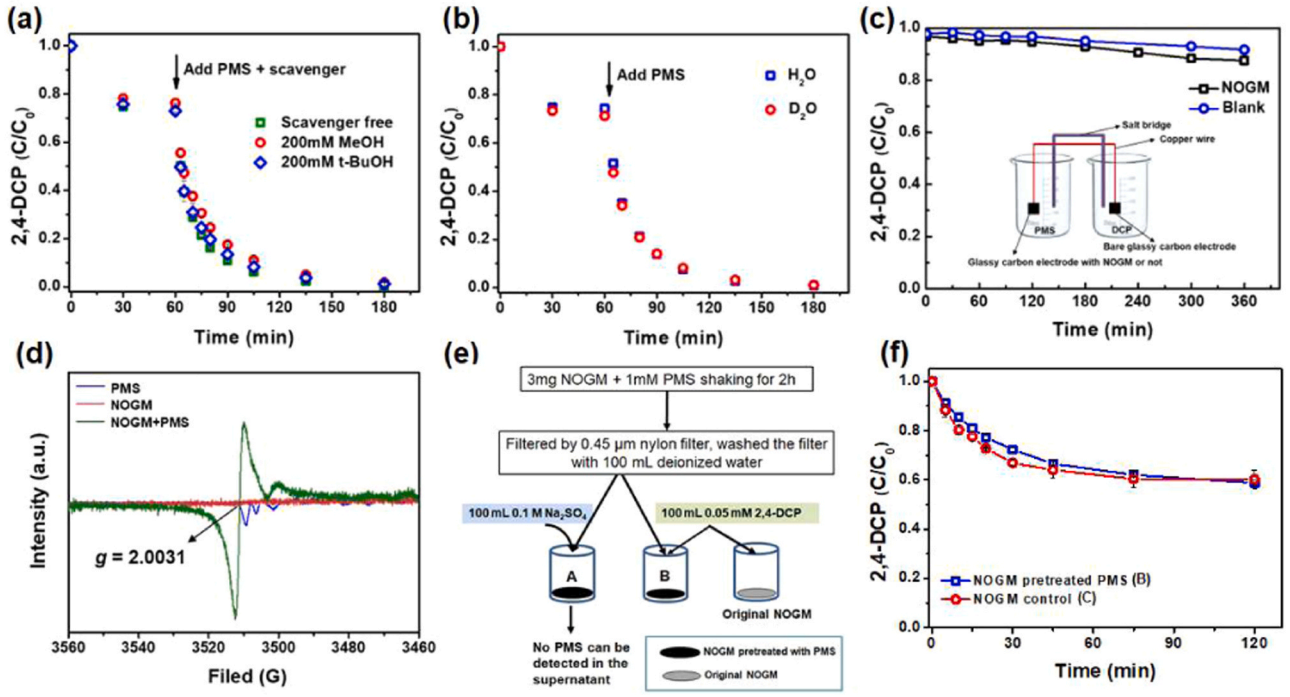

Fig. 2. Reactive species identification. (a) Scavenger experiments; (b) the effect of reaction solvents (H_2O and D_2O); $[2,4\text{-DCP}]_0 = 50$ μM, NOGM= 3 mg/100 mL, $[PMS]_0 = 1$ mM, pH= 7; (c) decay curves of 2,4-DCP in the electrochemical cell setup, $[2,4\text{-DCP}]_0 = 50$ μM, $[PMS]_0 = 1$ mM, pH= 7; (d) solid EPR spectra of PMS and mixture of oxone and NOGM; (e) experiment procedure of pre-treated with PMS; (f) 2,4-DCP degradation kinetic in (e), $[2,4\text{-DCP}]_0 = 50$ μM, NOGM= 3 mg/100 mL, $[PMS]_0 = 1$ mM, pH= 7.

69] can be observed in mixture of NOGM and PMS solid, reactive intermediates do not persist in measurable quantities (as 2,4-DCP decay) when PMS is washed away (Fgiure 2e and 2 f) nor NOGM pre-contact with PMS (Figs. 1d and 1e). If the surface is one-electron oxidized by PMS to give radicals, PMS would be one-electron reduced. A so-formed PMS radical anion would be highly unstable and decompose to oxyl radicals ($e^-_{aq} + PMS \rightarrow \cdot OH + SO_4^{2-}$, $8.4 \times 10^9\ M^{-1}s^{-1}$)(Resources), which do not participate according to the alcohol scavenging results. 5) PMS could form an "activated complex", as has been proposed. Its formation cannot be rate-limiting since the rate varies widely among the compounds tested (Fig. 1a). If its formation involves one electron transfer from the surface to PMS, it is hard to imagine a pathway that does not produce •OH and/or $SO_4\bullet^-$ as a result. The second through last points have not been fully considered in the past in evaluating the validity of surface-mediated PMS oxidations. Detailed results and discussion are in Text S5.

A final consideration is a two-electron (nucleophilic-electrophilic) mechanism involving active site(s) generated by PMS transformation of the surface or formation of a bound derivative of PMS that is more reactive than PMS itself. The observed high selectivity of catalysis argues in favor of such pathway.

3.2.2. Products identification

Degradation products of 2,4-DCP associated with the solid phase were determined via UPLC-TOF-MS/MS. We identified the following oligomer formulas in methanol extracts of the used catalyst: $C_{12}H_5Cl_4O_2$, $C_{12}H_7Cl_3O_3$, $C_{18}H_6Cl_6O_2$, $C_{18}H_7Cl_5O_2$, $C_{24}H_{10}Cl_8O$, $C_{24}H_8Cl_8O_3$. The MS spectra and suggested structures are given in Fig. S11. We could not determine the yields of these products. Formation of oligomers is usually attributed to prior generation of phenoxyl radicals that then couple through C-C or C-O bond-forming pathways [65]. XPS spectra of NOGM after degradation (NOGM-DCP-PMS) and used NOGM extracted by methanol (NOGM-DCP-PMS-Methanol) (Fig. S12) presented that there are some quinone groups on the products which is in accordance to the Fig. S11a. Oligomeric phenols have been found in many nonradical systems using persulfates as oxidant [27,45,60,65]. But, it is still unclear whether the oligomers originate from a main, non-radical pathway, or as side products resulting from a minor pathway that generates free radicals.

3.3. Examination of Surface Group Transformations by Raman, XPS, DRIFTS, and soft XAS spectroscopies

3.3.1. In-situ Raman

The Raman spectrum of Oxone® together with the calculated spectrum of HSO_5^-, appear in Fig. 3a. The peaks at 1060 cm^{-1} and 960 cm^{-1} correspond to S-O stretching vibrations in SO_4^{2-} and HSO_5^-. The peak at 886 cm^{-1} can be assigned to the peroxide (O-O) stretch in HSO_5^-. The Raman spectrum of a solid mixture of NOGM and PMS (Fig. 3b) gives a new peak at 816 cm^{-1}. Previous studies [32,44] attributed a Raman peak at 835 cm^{-1} in aqueous mixtures of PMS and carbocatalysts to an activated peroxo species, but did not assign a structure. It is reasonable to suppose that the peaks at 816 cm^{-1} and 835 cm^{-1} correspond to the O-O linkage of a PMS-transformed surface group or a PMS-derived species bound to the surface of NOGM. Possible structures of the latter and their calculated spectra are shown in Fig. S13-S15. Relative to the peak at 886 cm^{-1} of HSO_5^-, peaks for structures C−$OOSO_3^-$ in which C is a sp^2 carbon of an aromatic ring are red shifted or only slightly blue shifted (879–912 cm^{-1}; Figs. S13b, 13c, 13e). A stronger blue shift (to 810–860) is seen when C is a sp^3 carbon that bears one N or (especially) two N atoms. Peaks for organoperoxides C-OO-C, where C is sp^2 (aryl, alkene) or sp^3 (methyl) exist at 797- 813 nm (Figs. S14h-S14j). Hence, the peroxy groups detected in the NOGM/PMS mixture are most reasonably assigned to C_{sp3}-OO-SO_3^- groups. Organoperoxide groups are less easy to justify mechanistically, but we cannot rule them out.

3.3.2. Pre-contact experiments and corresponding XPS

Pre-contact experiments were carried out to explore possible active sites (see text S5 and Fig. 1d). NOGM pre-contacted with PMS (only) for

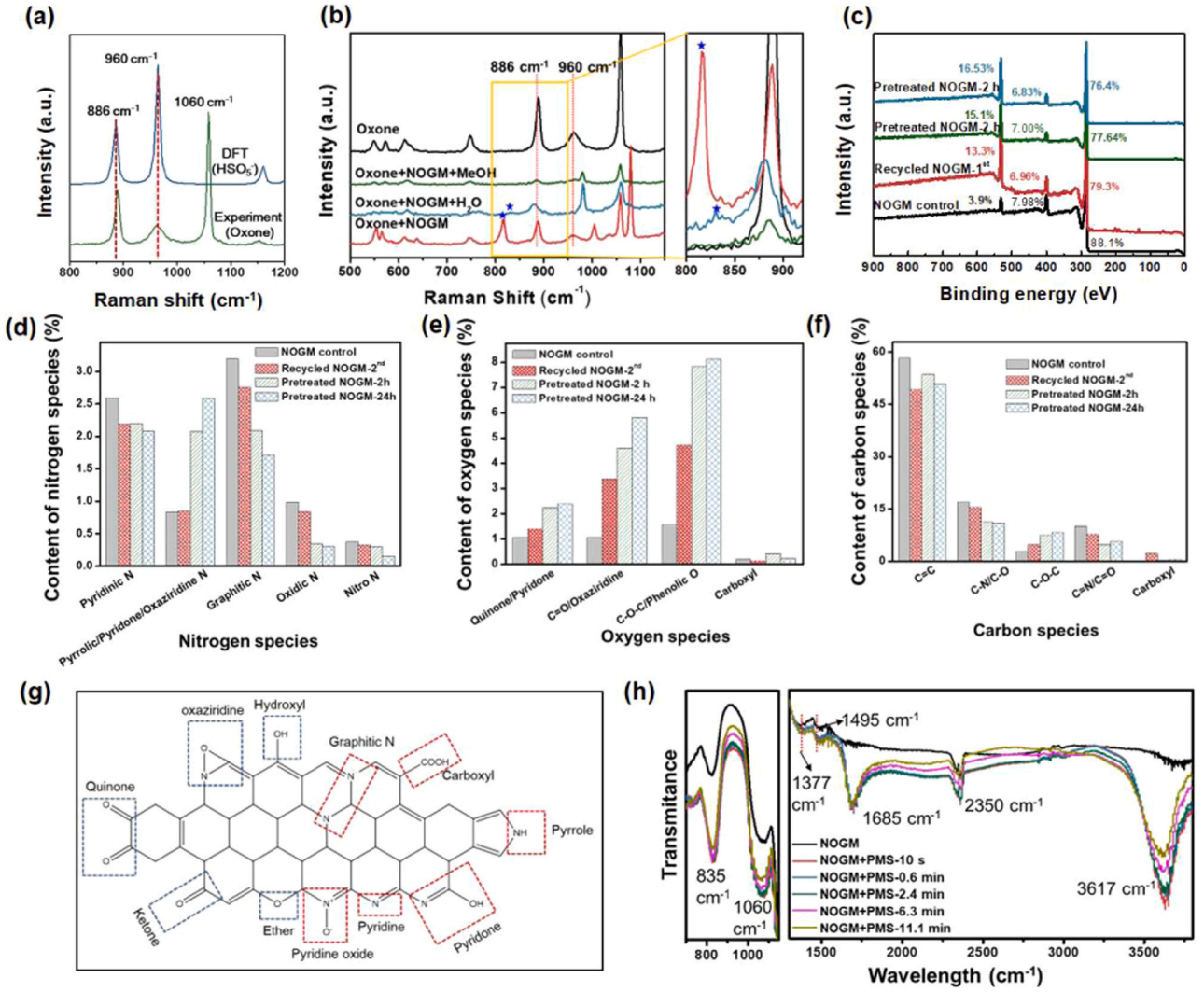

Fig. 3. (a) Raman spectra of HSO_5^- (calculated by density functional theory (DFT)) and oxone (experimental) (The peak at 960 cm^{-1} is the stretching vibration of S═O and S-O of HSO_5^-; the peak at 1060 cm^{-1} in oxone is the stretching vibration of S═O in SO_4^{2-} because oxone is a mixture of potassium salts of peroxymonosulfate and sulfate.); (b) in situ Raman spectra whole (left) and partial (right) in the PMS/NOGM system; (c) XPS survey; (d) content of each N species; (e) content of each O species; (f) content of each C species. Content of each species = ratio of specific species from peak fitting * content of element derived from XPS survey; (g) scheme of N, C, and O functionalities in NOGM; (h) in situ DRIFTS of NOGM reacted with PMS solution (high concentration) for different time (the double peaks at ~2350 cm^{-1} are the vibrations of C═O in CO_2).

2 or 24 h retained its graphene-like structure (SEM, Fig. S9), but showed a slight loss of defects (I_D/I_G; Fig. S10a) and a significant gain of impedance (EIS; Fig. S10b). It has been shown that defects like edges and vacancies can react with PMS [58,64]. These results, taken together, imply PMS decomposes and/or reacts with the surface, altering its physical properties and making it less catalytically active.

Spectra were compared for samples of NOGM that were either, taken through a typical single degradation cycle (1 mM PMS, 50 μM 2,4-DCP, 2 h) ("NOGM-control"), recycled one time ("NOGM-1st "), or pre-treated for 2 or 24 h prior to a single use ("Pretreated-NOGM-2 h" or "Pre-treated-NOGM-24 h"). The corresponding 2,4-DCP decay curves are given in Fig. S16). They reveal, once again, that NOGM loses activity with repeated use or pre-contact with PMS. The XPS survey (Fig. 3c) shows a large increase in O content and a small decrease in N content for all three treated samples relative to the NOGM-control. Fig. 3d,e,f show normalized peak abundance for XPS-assigned structures depicted in Fig. 3d. The actual deconvoluted spectra are in Fig. S17. Assignments are based on available databases.[26,31,70] For raw NOGM, peaks in the spectrum N1s can be assigned to: pyridine (398.9 eV); pyrrole or pyridone or oxaziridine N (400.1 eV); graphitic N (401.4 eV); pyridine N-oxide or quaternary ammonium (403.2 eV); and nitro (406.1 eV). The peaks in the O1s can be assigned to: quinone or pyridone (530.8 eV); C═O or oxaziridine (531.8 eV); ether or phenolic (533.1 eV); and carboxyl (536.1 eV). The peaks in the C1s can be assigned to: C═C (284.8 eV); C-O-C (287.9 eV); C-N or C-O (286.1 eV); and C═N or C═O (289.3 eV).

The XPS spectra, quantified in Fig. 3d,e,f, indicate major changes associated with PMS pre-contact (Fig. S16). The most conspicuous change in the N1s occurs for the pyrrole/pyridone peak, which triples in intensity. Other major changes occur in the pyridine-N-oxide/quaternary ammonium N, which declines by two-thirds, and the graphitic N (i.e., N at bridgehead positions), which declines by a third. The O1s spectrum shows increases in C═O/oxaziridine and ether/phenolic peaks, and decreases in quinone/pyridone and carboxylic peaks. The C1s spectrum shows a major increase in C-O-C, and minor decreases in C-N/C-O and C═N/C═O. The changes are greater for Pretreated-NOGM-2 h than Pretreated-NOGM-24 h. In general, the changes observed for NOGM-1st parallel those for Pretreated-NOGM-2 h and Pretreated-NOGM-24 h samples, but are weaker. This suggests that 2,4-DCP competes for sites that, in its absence, are chemically

transformed by PMS.

3.3.3. *In situ DRIFTS*

Spectra of NOGM contacted with aqueous PMS for different times up to 11 min appear in Fig. 3h. The peak at 3617 cm^{-1} is attributed to O-H stretch. A strong peak at 1685 cm^{-1} appeared within 10 s and hardly changed by 11.1 min. This peak is assigned to either the C-O stretch of C═O in an α,β-unsaturated ketone[5] or a pyridone [20]. Based on the XPS results, it is most likely a pyridone. Peaks at 1377 cm^{-1} and 1495 cm^{-1} are associated with symmetric and asymmetric stretching vibrations of N-O in nitro groups, respectively; they are strengthened with reaction time due presumable due to surface oxidation by PMS [2, 39]. The growing peak at 1060 cm^{-1} is attributed to C-O stretching and indicates introduction of hydroxyl and/or ether groups. The growing peak at 835 cm^{-1} is the out-of-plane flexing of C-H in aromatic rings.

3.3.4. *C K-edge, and N K-edge XAS spectra*

To directly observe the changes of functional groups on the surface of NOGM during its reaction with PMS and 2,4-DCP, X-ray absorption spectroscopy (XAS) was utilized, as shown in Fig. 4. The spectra of NOGM, NOGM reacted with PMS (NOGM-PMS), NOGM-PMS reacted with 2,4-DCP (NOGM-PMS-DCP) and CSOX were collected. We compared this with the XAS spectra of a commercially available oxaziridine compound, (1 R)-(−)-(10-camphorsulfonyl)oxaziridine (CSOX), depicted in Fig. 4a. The C K-edge XAS spectra, illustrated in Fig. 4a, revealed that NOGM displays three peaks at 285.4 eV, 288.3 eV, and 292.7 eV, corresponding to unoccupied π * , C-N bonding, and excited σ * states, respectively [19,72]. In contrast, CSOX shows a peak at 287.3 eV, attributed to the C-S σ * [37]. The reaction with PMS notably decreased the intensity of peak D in NOGM, suggesting a partial breakdown of the π-electron system (sp^2 hybridization). Unlike NOGM, NOGM-PMS exhibits two distinct peaks at 297.0 and 299.6 eV, which are also present in CSOX. These peaks likely represent the C-N and C-O structures in oxaziridines. The subsequent addition of 2,4-DCP reduced the intensity of these peaks, providing evidence for the interaction between oxaziridines and 2,4-DCP. The N K-edge XAFS spectra of NOGM and NOGM-PMS show peaks at 398.1 eV (peak A), 399.2–399.6 eV (peak B), 401.1–401.3 eV (peak C) and 407 eV (peak D), with peak D corresponding to the C-N σ * resonance [37]. Peaks B and C are linked to the π * features of pyridine-like and graphite-like N structures [37,38]. A noticeable increase in energy for peaks B indicates that pyridine and graphitic N were bound to electron-withdrawing groups [21]. The intensities of peaks A and B increased from NOGM to NOGM-PMS but decreased back to NOGM levels after adding 2,4-DCP, illustrating that the π * features of the pyridine-like structure were enhanced during the reaction between NOGM and PMS and altered during the reaction with 2,4-DCP. This also suggests that the pyridine-like structure could be a potential active sites.

3.4. *Examination of Specific Pathways*

Pathways **A** – **E** in Scheme 1 are offered to rationalize the spectroscopic changes. Paths **A** and **A′** involve nucleophilic attack of PMS on an imine-type edge-N to form initially a PMS adduct (**A-2, A′−2**) that decays to, respectively, a neutral and a charged oxaziridine group (**A-3, A′ 3**). The oxaziridine group can undergo rearrangement to a pyridone (**A-4** or else react with an organic compound, regenerating the starting imine. Path **B** is attack of PMS on a C═C bond in conjugation with a valley bridgehead (graphitic) N and leads to hydroxylation at the β or δ carbon (**B-3**). Path **C** is a two-electron oxidation of a keto-phenol ring system leading via intramolecular cyclization to an ether-keto system called a pyrone (**C-2**); such transformation has been proposed in activated carbons [28]. Path **D** is conversion of a quinone keto group to a dioxirane group (**D-2**). The dioxirane can either decompose to $^1O_2$ by reaction with excess PMS, or react directly with an organic compound, in either case regenerating the quinone. Path **E** represents PMS attack on pyridinic or pyrrolic N to form the N-oxide species (**E-2**).

Paths **A – E** are largely consistent with the XPS spectral changes after PMS treatment (Fig. 3d-f). Path **A** can explain, a) the increase in the N1s peak at 400 eV if that peak is attributed to pyridone and oxaziridine which come closely in the same place (399.5 eV) [4], rather than to pyrrole N (the synthesis of pyrrolic rings by PMS treatment is difficult to envision); and b) an increase in the O1s of the peak at 531.8 eV if it is attributed to oxaziridine O, which comes closely in the same place (531.6 eV) [4] as C═O. The ether/phenolic O at 533.3 eV can be rationalized by Path **B**, Path **C**, or both. Path **C** can also explain the increase in the C-O-C emission at 288 eV. Path **D** can account for the decrease in the peak at 531 eV if it is attributed to a quinone O. Paths **A** –

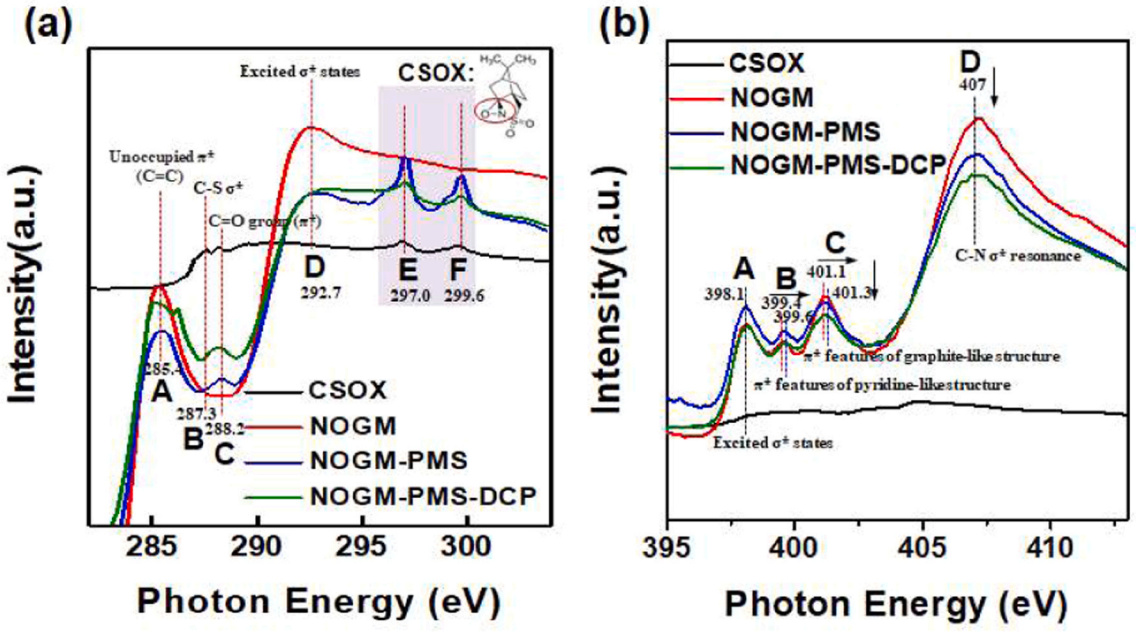

Fig. 4. C K-edge (a) and N K-edge (b) XAS spectra of NOGM, NOGM reacted with PMS solution (NOGM-PMS), NOGM reacted with PMS and 2,4-DCP (NOGM-PMS-DCP), and CSOX.

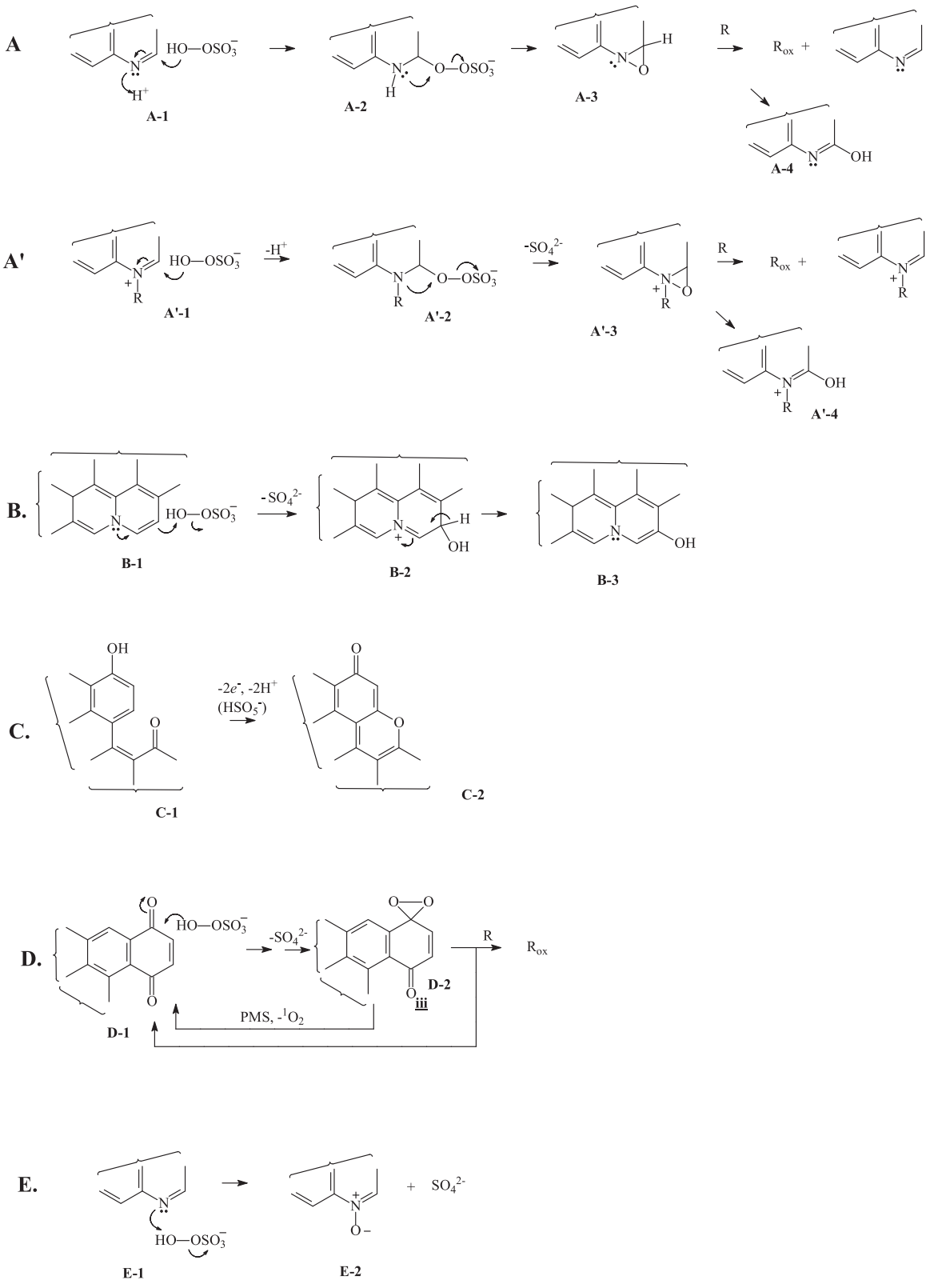

Scheme 1. Reaction pathways of PMS on NOGM surface groups.

E cannot explain the decreases in pyridinic N-oxide/quaternary ammonium N at 403.5 eV, the graphitic N at 401.1 eV, and the carboxylic O at 536 eV.

Represented in Scheme 1 are two functional groups known to be reactive towards organic compounds, oxaziridines and dioxiranes. Oxaziridines, which can be made by reactions of imines with peracids such as PMS, are useful oxidants in organic synthesis for a variety of functional group transformations. They react primarily as electrophilic O-atom transfer agents [51,7]. Dioxiranes derived from reaction of PMS with ketones are inherently strong oxidants that have been used in

organic synthesis [1,29,6]. Oxidation by dioxiranes occurs by a concerted electrophilic O-atom transfer from the dioxirane unit to a nucleophilic center on the target molecule. Oxaziridine and dioxirane groups react with a wide variety of organic compounds, listed in Text S4. Note that dioxiranes react with an excess of PMS to form $^1O_2$, which, however, has been ruled out for 2,4-DCP.

The XPS, Raman, DRIFTS, and X-ray absorption spectroscopic changes discussed above are consistent with PMS attack on surface moieties as a nucleophile towards imine (Paths A, A′; Scheme 1) and carbonyl (Path D) centers, as well as an electrophile towards bridgehead aromatic N groups (Path B), leading to identifiable surface transformations and generation of potentially short-lived reactive sites. PMS is known to behave as an electrophilic or nucleophilic oxidant depending on pH and target compound [34]. The nucleophilicity index of heterocyclic N computed by DFT (Table S4) follows the order: pyridone > graphitic N > pyrrolic N > pyridinic N. Except for pyridone, it increases with fused aromatic ring size. The degree of aromatic condensation grows with pyrolysis temperature [57], which may explain why the activity of N,O-doped carbons often increases with pyrolysis temperature [18,56,71].

4. Conclusion

This study touches on the fundamental side of the active sites, intermediates, and pathways of PMS activated by nitrogen-doped carbonaceous materials through theoretical deduction based on organic chemistry combining with a series of advanced characterizations. Results show that a two-electron (nucleophilic-electrophilic) mechanism but not reactive oxygen species nor direct one electron transfer, is the most likely oxidation mechanism. Imine-type edge-N (A-1 and A′−1) are possible active sites and oxaziridine (neutral and charged) is a possible active intermediate. Activation pathways of different sites with PMS are proposed and proved by XPS, DRIFITS, and C K-edge, and N K-edge XAS spectra. These pathways are much under-researched in heterogenous degradation systems with widely reported carbonaceous materials. Further investigation could include controlled synthesis of carbonaceous materials with higher content of imine-type edge-N (A-1 and A′−1).

CRediT authorship contribution statement

Wu Fengchang: Funding acquisition. **Dang Zhi:** Funding acquisition. **Zhao Qing:** Supervision, Funding acquisition. **Zhang Kejia:** Data curation. **Wang Chengjin:** Data curation. **Wang Zhengyang:** Data curation. **Wang Rui:** Data curation. **Yang Chen:** Project administration, Funding acquisition. **Yang Yi:** Methodology. **Yang Jingjing:** Writing – review & editing, Writing – original draft, Visualization, Software, Methodology, Investigation, Formal analysis, Data curation, Conceptualization. **Pignatello Joseph:** Writing – review & editing, Validation, Supervision, Resources, Project administration, Methodology, Investigation, Funding acquisition, Formal analysis.

Declaration of Competing Interest

The authors declare that they have no known competing financial interests or personal relationships that could have appeared to influence the work reported in this paper.

Data Availability

Data will be made available on request.

Acknowledgements

This research was supported by the National Natural Science Foundation of China (42307318, 42077337, 42022056), GDAS' Project of Science and Technology Development (2020GDASYL-20200101002, 2022GDASZH-2022010105), and the U.S. Department of Agriculture, National Institute of Food and Agriculture (1018681). The numerical calculations in this paper have been done on the supercomputing systems in the Supercomputing Center of University of Science and Technology of China. Soft X-ray adsorption measurements were conducted at Soft X-Ray Magnetic Circular Dichroism Endstation (SXMCD), National Synchrotron Radiation Laboratory, Hefei (China).

Appendix A. Supporting information

Supplementary data associated with this article can be found in the online version at doi:10.1016/j.apcatb.2024.123793.

References

[1] W. Adam, R. Curci, J.O. Edwards, Dioxiranes: a new class of powerful oxidants, Acc. Chem. Res. 22 (6) (1989) 205–211.
[2] E. Bamberger, R. Seligman, Oxydation aliphatischer Basen vom Typus: C.NH2, Ber. der Dtsch. Chem. Ges. 36 (1) (1903) 685–700.
[3] J. Chen, L. Zhang, T. Huang, W. Li, Y. Wang, Z. Wang, Decolorization of azo dye by peroxymonosulfate activated by carbon nanotube: Radical versus non-radical mechanism, J. Hazard. Mater. 320 (2016) 571–580.
[4] D.R. Crist, G.J. Jordan, J.A. Hashmall, Oxaziridine-silver fluoborate complexes. Site of complexation by carbon-13 nuclear magnetic resonance and x-ray photoelectron spectroscopy, J. Am. Chem. Soc. 96 (15) (1974) 4927–4932.
[5] N.H. Cromwell, F.A. Miller, A.R. Johnson, R.L. Frank, D.J. Wallace, Infrared Spectra of Amino-substituted α,β-Unsaturated Ketones, J. Am. Chem. Soc. 71 (10) (1949) 3337–3342.
[6] R. Curci, A. Dinoi, M.F. Rubino, Dioxirane oxidations: taming the reactivity-selectivity principle, Pure Appl. Chem. 67 (5) (1995) 811–822.
[7] F.A. Davis, A.C. Sheppard, Applications of oxaziridines in organic synthesis, Tetrahedron 45 (18) (1989) 5703–5742.
[8] J. Dou, Y. Tang, Z. Lu, G. He, J. Xu, Y. He, Neglected but efficient electron utilization driven by biochar-coactivated phenols and peroxydisulfate: polyphenol accumulation rather than mineralization, Environ. Sci. Technol. 57 (14) (2023) 5703–5713.
[9] X. Duan, H. Sun, S. Wang, Metal-free carbocatalysis in advanced oxidation reactions, Acc. Chem. Res. 51 (3) (2018) 678–687.
[10] X. Duan, H. Sun, Y. Wang, J. Kang, S. Wang, N-doping-induced nonradical reaction on single-walled carbon nanotubes for catalytic phenol oxidation, ACS Catal. 5 (2) (2015) 553–559.
[11] X. Duan, Z. Ao, H. Sun, L. Zhou, G. Wang, S. Wang, Insights into N-doping in single-walled carbon nanotubes for enhanced activation of superoxides: a mechanistic study, Chem. Commun. 51 (83) (2015) 15249–15252.
[12] X. Duan, Z. Ao, H. Sun, S. Indrawirawan, Y. Wang, J. Kang, F. Liang, Z.H. Zhu, S. Wang, Nitrogen-doped graphene for generation and evolution of reactive radicals by metal-free catalysis, ACS Appl. Mater. Interfaces. 7 (7) (2015) 4169–4178.
[13] X. Duan, C. Su, L. Zhou, H. Sun, A. Suvorova, T. Odedairo, Z. Zhu, Z. Shao, S. Wang, Surface controlled generation of reactive radicals from persulfate by carbocatalysis on nanodiamonds, Appl. Catal. B-Environ. 194 (2016) 7–15.
[14] G. Fang, C. Liu, J. Gao, D.D. Dionysiou, D. Zhou, Manipulation of persistent free radicals in biochar to activate persulfate for contaminant degradation, Environ. Sci. Technol. 49 (9) (2015) 5645–5653.
[15] Y. Fu, Y. Yan, Z. Wei, R. Spinney, D.D. Dionysiou, D. Vione, M. Liu, R. Xiao, Overlooked transformation of nitrated polycyclic aromatic hydrocarbons in natural waters: role of self-photosensitization, Environ. Sci. Technol. 57 (26) (2023) 9832–9842.
[16] C. Guan, J. Jiang, S. Pang, C. Luo, J. Ma, Y. Zhou, Y. Yang, Oxidation kinetics of bromophenols by nonradical activation of peroxydisulfate in the presence of carbon nanotube and formation of brominated polymeric products, Environ. Sci. Technol. 51 (18) (2017) 10718–10728.
[17] D. Guo, R. Shibuya, C. Akiba, S. Saji, T. Kondo, J. Nakamura, Active sites of nitrogen-doped carbon materials for oxygen reduction reaction clarified using model catalysts, Science 351 (6271) (2016) 361–365.
[18] P. Hu, H. Su, Z. Chen, C. Yu, Q. Li, B. Zhou, P.J.J. Alvarez, M. Long, Selective degradation of organic pollutants using an efficient metal-free catalyst derived from carbonized polypyrrole via peroxymonosulfate activation, Environ. Sci. Technol. 51 (19) (2017) 11288–11296.
[19] K. Kaznacheyev, A. Osanna, C. Jacobsen, O. Plashkevych, O. Vahtras, Ågren, V. Carravetta, A.P. Hitchcock, Innershell absorption spectroscopy of amino acids, J. Phys. Chem. A 106 (13) (2002) 3153–3168.
[20] G.H. Keller, L. Bauer, C.L. Bell, Infrared spectra of 2-pyridone-16O and 2-pyridone-18O, Can. J. Chem. (1968).
[21] K.G. Latham, W.M. Dose, J.A. Allen, S.W. Donne, Nitrogen doped heat treated and activated hydrothermal carbon: NEXAFS examination of the carbon surface at different temperatures, Carbon 128 (2018) 179–190.
[22] H. Lee, H.-J. Lee, J. Jeong, J. Lee, N.-B. Park, C. Lee, Activation of persulfates by carbon nanotubes: Oxidation of organic compounds by nonradical mechanism, Chem. Eng. J. 266 (2015) 28–33.

[23] H. Lee, H.-I. Kim, S. Weon, W. Choi, Y.S. Hwang, J. Seo, C. Lee, J.-H. Kim, Activation of persulfates by graphitized nanodiamonds for removal of organic compounds, Environ. Sci. Technol. 50 (18) (2016) 10134–10142.
[24] P. Liang, C. Zhang, X. Duan, H. Sun, S. Liu, M.O. Tade, S. Wang, N-doped graphene from metal-organic frameworks for catalytic oxidation of p-hydroxylbenzoicl acid: N-functionality and mechanism, ACS Sustain. Chem. Eng. 5 (3) (2017) 2693–2701.
[25] J. Liu, W. Li, L. Duan, X. Li, L. Ji, Z. Geng, K. Huang, L. Lu, L. Zhou, Z. Liu, W. Chen, L. Liu, S. Feng, Y. Zhang, A graphene-like oxygenated carbon nitride material for improved cycle-life lithium/sulfur batteries, Nano Lett. 15 (8) (2015) 5137–5142.
[26] S. Men, P. Licence, H. Luo, S. Dai, Tuning the cation–anion interactions by methylation of the pyridinium cation: an X-ray photoelectron spectroscopy study of picolinium ionic liquids, J. Phys. Chem. B 124 (30) (2020) 6657–6663.
[27] J. Miao, W. Geng, P.J.J. Alvarez, M. Long, 2D N-doped porous carbon derived from polydopamine-coated graphitic carbon nitride for efficient nonradical activation of peroxymonosulfate, Environ. Sci. Technol. 54 (13) (2020) 8473–8481.
[28] M.A. Montes-Moran, D. Suarez, J.A. Menendez, E. Fuente, On the nature of basic sites on carbon surfaces: an overview, Carbon 42 (7) (2004) 1219–1225.
[29] R.W. Murray, R. Jeyaraman, Dioxiranes: synthesis and reactions of methyldioxiranes, J. Org. Chem. 50 (16) (1985) 2847–2853.
[30] W.-D. Oh, G. Lisak, R.D. Webster, Y.-N. Liang, A. Veksha, A. Giannis, J.G.S. Moo, J.-W. Lim, T.-T. Lim, Insights into the thermolytic transformation of lignocellulosic biomass waste to redox-active carbocatalyst: durability of surface active sites, Appl. Catal. B-Environ. 233 (2018) 120–129.
[31] J.R. Pels, F. Kapteijn, J.A. Moulijn, Q. Zhu, K.M. Thomas, Evolution of nitrogen functionalities in carbonaceous materials during pyrolysis, Carbon 33 (11) (1995) 1641–1653.
[32] W. Ren, G. Nie, P. Zhou, H. Zhang, X. Duan, S. Wang, The intrinsic nature of persulfate activation and N-doping in carbocatalysis, Environ. Sci. Technol. 54 (10) (2020) 6438–6447.
[33] W. Ren, L. Xiong, G. Nie, H. Zhang, X. Duan, S. Wang, Insights into the electron-transfer regime of peroxydisulfate activation on carbon nanotubes: the role of oxygen functional groups, Environ. Sci. Technol. 54 (2) (2020) 1267–1275.
[34] M. Ruiz, Y. Yang, C.A. Lochbaum, D.G. Delafield, J.J. Pignatello, L. Li, J. A. Pedersen, Peroxymonosulfate oxidizes amino acids in water without activation, Environ. Sci. Technol. 53 (18) (2019) 10845–10854.
[35] P. Shao, J. Tian, F. Yang, X. Duan, S. Gao, W. Shi, X. Luo, F. Cui, S. Luo, S. Wang, Identification and regulation of active sites on nanodiamonds: establishing a highly efficient catalytic system for oxidation of organic contaminants, Adv. Funct. Mater. 28 (13) (2018) 1705295.
[36] P. Shao, Y. Jing, X. Duan, H. Lin, L. Yang, W. Ren, F. Deng, B. Li, X. Luo, S. Wang, Revisiting the graphitized nanodiamond-mediated activation of peroxymonosulfate: singlet oxygenation versus electron transfer, Environ. Sci. Technol. 55 (23) (2021) 16078–16087.
[37] I. Shimoyama, G. Wu, T. Sekiguchi, Y. Baba, Evidence for the existence of nitrogen-substituted graphite structure by polarization dependence of near-edge x-ray-absorption fine structure, Phys. Rev. B 62 (10) (2000) R6053–R6056.
[38] I. Shimoyama, G. Wu, T. Sekiguchi, Y. Baba, Study of electronic structure of graphite-like carbon nitride, J. Electron. Spectrosc. Relat. Phenom. 114-116 (2001) 841–848.
[39] E.A. Skrotzki, J.K. Vandavasi, S.G. Newman, Ozone-mediated amine oxidation and beyond: a solvent-free, flow-chemistry approach, J. Org. Chem. 86 (20) (2021) 14169–14176.
[40] H. Sun, S. Liu, G. Zhou, H.M. Ang, M.O. Tade, S. Wang, Reduced graphene oxide for catalytic oxidation of aqueous organic pollutants, ACS Appl. Mater. Inter. 4 (10) (2012) 5466–5471.
[41] P. Sun, H. Liu, M. Feng, L. Guo, Z. Zhai, Y. Fang, X. Zhang, V.K. Sharma, Nitrogen-sulfur co-doped industrial graphene as an efficient peroxymonosulfate activator: singlet oxygen-dominated catalytic degradation of organic contaminants, Appl. Catal. B-Environ. 251 (2019) 335–345.
[42] L. Tang, Y. Liu, J. Wang, G. Zeng, Y. Deng, H. Dong, H. Feng, J. Wang, B. Peng, Enhanced activation process of persulfate by mesoporous carbon for degradation of aqueous organic pollutants: electron transfer mechanism, Appl. Catal. B-Environ. 231 (2018) 1–10.
[43] A. Valavanidis, N. Iliopoulos, G. Gotsis, K. Fiotakis, Persistent free radicals, heavy metals and PAHs generated in particulate soot emissions and residue ash from controlled combustion of common types of plastic, J. Hazard. Mater. 156 (1) (2008) 277–284.
[44] Z. Wan, Z. Xu, Y. Sun, M. He, D. Hou, X. Cao, D.C.W. Tsang, Critical impact of nitrogen vacancies in nonradical carbocatalysis on nitrogen-doped graphitic biochar, Environ. Sci. Technol. 55 (10) (2021) 7004–7014.
[45] C. Wang, S.-Y. Jia, Y. Han, Y. Li, Y. Liu, H.-T. Ren, S.-H. Wu, X. Han, Selective oxidation of various phenolic contaminants by activated persulfate via the hydrogen abstraction pathway, ACS EST Eng. 1 (9) (2021) 1275–1286.
[46] H. Wang, W. Guo, B. Liu, Q. Wu, H. Luo, Q. Zhao, Q. Si, F. Sseguya, N. Ren, Edge-nitrogenated biochar for efficient peroxydisulfate activation: An electron transfer mechanism, Water Res. 160 (2019) 405–414.
[47] J. Wang, S. Wang, Activation of persulfate (PS) and peroxymonosulfate (PMS) and application for the degradation of emerging contaminants, Chem. Eng. J. 334 (2018) 1502–1517.
[48] J. Wang, J. Yang, S. Liu, C. Yang, Q. Yang, Z. Dang, Probing the activation mechanism of nitrogen-doped carbonaceous materials for persulfates: Based on the differences between peroxymonosulfate and peroxydisulfate, Environ. Pollut. 329 (2023) 121685.
[49] R. Wang, S. Zhang, H. Chen, Z. He, G. Cao, K. Wang, F. Li, N. Ren, D. Xing, S.-H. Ho, Enhancing biochar-based nonradical persulfate activation using data-driven techniques, Environ. Sci. Technol. 57 (9) (2023) 4050–4059.
[50] Y. Wang, X. Duan, Y. Xie, H. Sun, S. Wang, Nanocarbon-based catalytic ozonation for aqueous oxidation: engineering defects for active sites and tunable reaction pathways, ACS Catal. 10 (22) (2020) 13383–13414.
[51] K.S. Williamson, D.J. Michaelis, T.P. Yoon, Advances in the chemistry of oxaziridines, Chem. Rev. 114 (16) (2014) 8016–8036.
[52] L. Won Jun, L. Joonwon, K. Sang Ouk, Nitrogen dopants in carbon nanomaterials: defects or a new opportunity? Small Methods 1 (1-2) (2017) 1600014.
[53] X. Wu, J.-H. Kim, Outlook on single atom catalysts for persulfate-based advanced oxidation, ACS EST Eng. 2 (10) (2022) 1776–1796.
[54] J. Xu, Y. Yao, C. Zhu, L. Lu, Q. Fang, Z. He, S. Song, B. Chen, Y. Shen, Unveiling enhanced electron-mediated peroxymonosulfate activation for degradation of emerging organic pollutants, Appl. Catal. B-Environ. 341 (2024) 123356.
[55] Y. Yan, Z. Wei, X. Duan, M. Long, R. Spinney, D.D. Dionysiou, R. Xiao, P.J. J. Alvarez, Merits and limitations of radical vs. nonradical pathways in persulfate-based advanced oxidation processes, Environ. Sci. Technol. 57 (33) (2023) 12153–12179.
[56] J. Yang, J. Wang, H. Li, Y. Deng, C. Yang, Q. Zhao, Z. Dang, Nitrogen-doped biochar as peroxymonosulfate activator to degrade 2,4-dichlorophenol: Preparation, properties and structure–activity relationship, J. Hazard. Mater. 424 (2022) 127743.
[57] J. Yang, J.J. Pignatello, K. Yang, W. Wu, G. Lu, L. Zhang, C. Yang, Z. Dang, Adsorption of organic compounds by biomass chars: direct role of aromatic condensation (ring cluster size) revealed by experimental and theoretical studies, Environ. Sci. Technol. 55 (3) (2021) 1594–1603.
[58] S. Yang, S. Xu, J. Tong, D. Ding, G. Wang, R. Chen, P. Jin, X.C. Wang, Overlooked role of nitrogen dopant in carbon catalysts for peroxymonosulfate activation: Intrinsic defects or extrinsic defects? Appl. Catal. B-Environ. 295 (2021) 120291.
[59] Y. Yang, G. Banerjee, G.W. Brudvig, J.-H. Kim, J.J. Pignatello, Oxidation of organic compounds in water by unactivated peroxymonosulfate, Environ. Sci. Technol. 52 (10) (2018) 5911–5919.
[60] Y. Yang, P. Zhang, K. Hu, P. Zhou, Y. Wang, A.H. Asif, X. Duan, H. Sun, S. Wang, Crystallinity and valence states of manganese oxides in Fenton-like polymerization of phenolic pollutants for carbon recycling against degradation, Appl. Catal. B-Environ. 315 (2022) 121593.
[61] E.-T. Yun, H.-Y. Yoo, H. Bae, H.-I. Kim, J. Lee, Exploring the role of persulfate in the activation process: radical precursor versus electron acceptor, Environ. Sci. Technol. 51 (17) (2017) 10090–10099.
[62] E.-T. Yun, J.H. Lee, J. Kim, H.-D. Park, J. Lee, Identifying the nonradical mechanism in the peroxymonosulfate activation process: singlet oxygenation versus mediated electron transfer, Environ. Sci. Technol. 52 (12) (2018) 7032–7042.
[63] E.-T. Yun, G.-H. Moon, H. Lee, T.H. Jeon, C. Lee, W. Choi, J. Lee, Oxidation of organic pollutants by peroxymonosulfate activated with low-temperature-modified nanodiamonds: understanding the reaction kinetics and mechanism, Appl. Catal. B-Environ. 237 (2018) 432–441.
[64] W. Zhang, Y. Li, X. Fan, F. Zhang, G. Zhang, Y.-A. Zhu, W. Peng, S. Wang, X. Duan, Synergy of nitrogen doping and structural defects on hierarchically porous carbons toward catalytic oxidation via a non-radical pathway, Carbon 155 (2019) 268–278.
[65] Y.-J. Zhang, G.-X. Huang, L.R. Winter, J.-J. Chen, L. Tian, S.-C. Mei, Z. Zhang, F. Chen, Z.-Y. Guo, R. Ji, Y.-Z. You, W.-W. Li, X.-W. Liu, H.-Q. Yu, M. Elimelech, Simultaneous nanocatalytic surface activation of pollutants and oxidants for highly efficient water decontamination, Nat. Commun. 13 (1) (2022) 3005.
[66] C. Zhao, S. Zhang, M. Han, X. Zhang, Y. Liu, W. Li, C. Chen, G. Wang, H. Zhang, H. Zhao, Ambient electrosynthesis of ammonia on a biomass-derived nitrogen-doped porous carbon electrocatalyst: contribution of pyridinic nitrogen, ACS Energy Lett. 4 (2) (2019) 377–383.
[67] Y. Zhen, S. Zhu, Z. Sun, Y. Tian, Z. Li, C. Yang, J. Ma, Identifying the persistent free radicals (PFRs) formed as crucial metastable intermediates during peroxymonosulfate (PMS) activation by N-doped carbonaceous materials, Environ. Sci. Technol. 55 (13) (2021) 9293–9304.
[68] Y. Zhou, J. Jiang, Y. Gao, S.-Y. Pang, Y. Yang, J. Ma, J. Gu, J. Li, Z. Wang, L.-H. Wang, L.-P. Yuan, Y. Yang, Activation of peroxymonosulfate by phenols: Important role of quinone intermediates and involvement of singlet oxygen, Water Res 125 (2017) 209–218.
[69] K. Zhu, H. Jia, S. Zhao, T. Xia, X. Guo, T. Wang, L. Zhu, Formation of Environmentally Persistent Free Radicals on Microplastics under Light Irradiation, Environ. Sci. Technol. 53 (14) (2019) 8177–8186.
[70] Q. Zhu, S.L. Money, A.E. Russell, K.M. Thomas, Determination of the fate of nitrogen functionality in carbonaceous materials during pyrolysis and combustion using X-ray absorption near edge structure spectroscopy, Langmuir 13 (7) (1997) 2149–2157.
[71] S. Zhu, X. Huang, F. Ma, L. Wang, X. Duan, S. Wang, Catalytic removal of aqueous contaminants on N-doped graphitic biochars: Inherent roles of adsorption and nonradical mechanism, Environ. Sci. Technol. 52 (15) (2018) 8649–8658.
[72] Y. Zubavichus, A. Shaporenko, M. Grunze, M. Zharnikov, Innershell absorption spectroscopy of amino acids at all relevant absorption edges, J. Phys. Chem. A 109 (32) (2005) 6998–7000.